A Rhombohedral Phase of Lipid Containing a Membrane Fusion Intermediate Structure

Lin Yang* and Huey W. Huang†
*National Synchrotron Light Source, Brookhaven National Laboratory, Upton, New York 11973;
and †Department of Physics & Astronomy, Rice University, Houston, Texas, 77251, USA

ABSTRACT We constructed the electron density distribution from the x-ray diffraction of a phase of phospholipid that exhibited rhombohedral symmetry. To determine the phases of the diffraction amplitudes, we first extended the well-known one-dimensional swelling method for planar bilayers to a three-dimensional method applicable to a layered system containing in-plane structures, such as rhombohedral structures. The complete phase determination was accomplished by a combination of the swelling method and Luzzati's pattern recognition method. The constructed electron density distribution showed that in each unit cell, two apposed monolayers merged across the water layer and developed into an hourglass structure consistent with a postulated membrane fusion intermediate state called a stalk. The observation of the stalk structure lends a strong support to the stalk hypothesis for membrane fusion and opens a way to measure the structural parameters in the fusion pathway.

INTRODUCTION

Diphytanoyl (3,7,11,15-tetramethylhexadecanoic) phosphatidylcholine (DPhPC) was found to exhibit a structure of rhombohedral symmetry between a lamellar phase and an inverted hexagonal phase as a function of hydration. In this paper we report the x-ray experiment that recorded the diffraction patterns of rhombohedral symmetry and the subsequent reconstruction of the electron density distribution from the data. We made use of a small range of hydration in which the rhombohedral structure existed, and applied a swelling method to help determine the relative phases of the diffraction peaks along the crystal axis perpendicular to the hexagonal base. Together with Luzzati's pattern recognition method, we determined the most reasonable phases for the diffraction amplitudes and reconstructed the electron density distribution of the rhombohedral phase. The density distribution contains a structure resembling the postulated intermediate state for membrane fusion (preliminary result published in Yang and Huang, 2002). Membrane fusion involves the merger of two phospholipid bilayers. The widely accepted model for membrane fusion is built upon the hypothesis that there is an intermediate state in which the two contacting monolayers become continuous via an hourglass structure called a stalk (Gingell and Ginsberg, 1978; Markin et al., 1984; Siegel, 1993; 1999; Lentz et al., 2000; Brunger, 2001; Kuzmin, et al., 2001; Kozlovsky and Kozlov, 2002; Markin and Albanesi, 2002; Lentz et al., 2002). This structure has not been observed by experiment so far. However, many efforts have been made to estimate the free energy for such a state (Markin et al., 1984; Siegel, 1993, 1999; Kuzmin, et al., 2001; Kozlovsky and Kozlov, 2002; Markin and Albanesi, 2002; Lentz et al., 2002). Theoretical estimates naturally depend on many assumed parameters, such as the size and shape of the stalk, the bending rigidity and spontaneous curvature of lipid monolayer, and whether the lipid is of single or multiple components. The discovery of the stalk structure in a stable phase opens a way to experimentally measure some of these parameters. The experiment can also be expanded to include proteins or peptides in this new phase of lipid to change the parameters of the stalk and to estimate the energy of the stalk formation.

To understand this new phase of lipid, it is useful to know how it was discovered. For the past several years, we have been studying antimicrobial peptides that are capable of forming transmembrane pores in lipid bilayers. To observe the transmembrane pores, we prepared lipid samples containing peptides as parallel layers intercalated with water. With water replaced by D_2O, neutron scattering with the scattering vector oriented in the plane of bilayers detected the transmembrane D_2O columns. The data were consistent with in-plane scattering by randomly distributed (or freely diffusing) transmembrane pores with mutual hard-core exclusion (He et al., 1995, 1996; Ludtke et al., 1996). A subsequent out-of-plane diffraction study showed that the in-plane positions of the pores in lipid bilayers were uncorrelated between adjacent bilayers (Yang et al., 1998, 1999). This was the result from fully hydrated multilayers. However, when the hydration level was reduced to less than full, the out-of-plane diffraction profile of the in-plane scattering peak indicated that the in-plane positions of the pores became correlated between adjacent bilayers (Yang et al., 1998, 1999). When we further manipulated the temperature and hydration of the multilayer samples, we succeeded in crystallizing the transmembrane pores in the multilayers (Yang et al., 2000). In one of the crystalline phases, the pores were distributed on a regular hexagonal lattice in each bilayer, and the layers were stacked in the ABCABC... sequence (Kittel, 1971). We called this the hexagonal ABC stacking, although unlike close-packed

Submitted August 22, 2002, and accepted for publication November 11, 2002.

Address reprint request to Dr. Huey W. Huang, Department of Physics & Astronomy, Rice University, Houston, TX 77251-1892. Tel.: 713-348-4899; Fax: 713-348-4150; E-mail: hwhuang@rice.edu.

0006-3495/03/03/1808/10 $2.00

spheres our lattice was not cubic, because the stacking distance was not geometrically related to the hexagonal size. The symmetry of the diffraction patterns was rhombohedral, space group $R\bar{3}$. One of our recent projects was to make use of the rhombohedral crystals to construct the electron density profile of the transmembrane pores. It was during such an experiment, we discovered that, to our surprise, a pure lipid also exhibited a rhombohedral phase.

The lipid was DPhPC, a modification of the well-known dipalmitoyl phosphatidylcholine (DPPC) with four methyl groups attached to each acyl chain at the carbon atom 3, 7, 11, and 15. DPhPC is characterized by its bulky, disordered chains. Consequently the lipid has a small ratio of cross sections between the headgroup and the chains (A_{hg}/A_{ch}). If DPPC monolayers have a zero spontaneous curvature, DPhPC has a negative one. In our previous studies (see Huang, 2000), DPhPC was an important lipid bilayer that was used to observe the transition of membrane-active peptides from a state of embedding in the headgroup region to a state of forming transmembrane pores, again due to its small A_{hg}/A_{ch}.

DPhPC multilayers were prepared as a thin film on a silicon nitride substrate. X-ray diffraction from DPhPC multilayers was recorded as a function of temperature and the degree of hydration of the sample. The latter was controlled by the ambient relative humidity in the sample chamber (Yang et al., 2000). Three phases were identified by their diffraction patterns within the range of 20°C to 30°C and relative humidity 50%–100%: a lamellar phase, a rhombohedral (hexagonal ABC stacking) phase, and a two-dimensional hexagonal phase. The lamellar phase is the familiar fluid phase of lipid bilayers that was discussed in Hung et al (2000). The two-dimensional hexagonal phase is the inverted hexagonal (H_{II}) phase (Gruner, 1989; Turner and Gruner, 1992). In this paper we will concentrate on the analysis of the rhombohedral phase. We will determine the phases of the diffraction patterns by extending a well-known one-dimensional swelling method to three dimensions and making use of Luzzati's pattern recognition method (Mariani et al., 1988). We will then discuss the electron density distribution in the unit cell that contains a stalk structure.

EXPERIMENT

Sample preparation and experimental setup

1,2-Diphytanoyl-*sn*-glycero-3-phosphatidylcholine (DPhPC) was purchased from Avanti Polar Lipids (Alabaster, AL) and used as delivered. Aligned multilayer samples were prepared by direct deposition of lipid from an organic solution onto a flat substrate. To ensure good layer alignment, the lipid amount was limited to $<\sim 0.5$ mg/cm^2. The organic solvent was a trifluoroethanol (TFE)-chloroform mixture. The ratio of trifluoroethanol to chloroform was varied to give optimal membrane alignment on the substrate (Ludtke et al., 1995). The organic solvent was removed in vacuum or evaporated in open air. The deposit was then hydrated with saturated water vapor at room temperature. Under this condition, the lipid spontaneously formed a stack of hydrated bilayers parallel to the substrate (Ludtke et al., 1995; He et al., 1996).

To allow for transmission diffraction, we used silicon nitrite windows (Silson Ltd., UK) as the substrate. The thickness of the window was 100 nm, which allowed for ~99% transmission of 8 keV x rays at 30° incident angle. The dimension of the window was 1.0 mm (vertical) × 3.0 mm (horizontal), and the footprint of the incident x ray in the transmission geometry was ~0.5 mm (vertical) × 1.0 mm (horizontal). The window was supported by a silicon frame.

Fig. 1 shows the experimental setup that was used to measure the diffraction patterns from aligned multilayer samples, at the beamline X21 of the National Synchrotron Light Source, Brookhaven National Laboratory (Upton, NY). The x-ray beam was collimated by two sets of slits before a sample chamber, resulting in a beam size of ~0.5 mm × ~0.5 mm at the sample. A helium beam path between the sample chamber and a MarCCD detector (MAR USA, Evanston, IL) was used to reduce the scattering by air. A beam stop and an attenuator were glued to a kapton film covering the CCD detector. The attenuator (a stack of aluminum foils) reduced the intensity of the first few orders of reflections off the crystal planes parallel to the substrate to avoid saturating the pixels on the CCD detector.

The temperature of the sample and the relative humidity of the surrounding air were controlled inside the sample chamber. The sample was attached to a temperature-controlled aluminum mount by heat-sink paste. The sample chamber could be rotated to alter the incident angle for both reflective and transmissive diffraction. Transmissive diffraction was achieved by an illuminating x ray from the backside of the substrate through a hole in the sample mount. Directly facing the sample surface was a water reservoir, where the water temperature was adjusted to vary the relative humidity inside the sample chamber. A temperature transducer (AD590, Analog Devices, Norwood, MA) and a relative humidity sensor (HC-600, Ohmic, Easton, MD) were mounted close to the sample to monitor the sample condition. The outputs from the sensing elements were fed to PID feedback control circuits, which in turn powered two sets of Peltier modules (Melcor, Trenton, NJ), one for heating or cooling the sample and another for

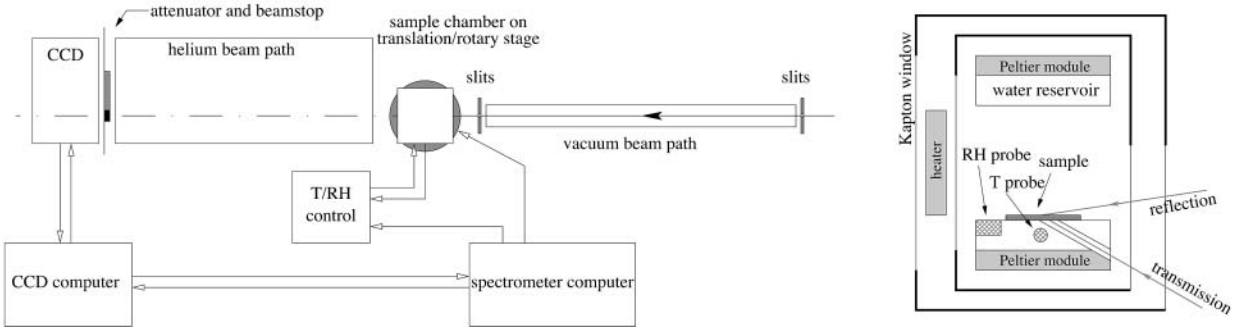

FIGURE 1 The experimental setup and the concept of the sample chamber. The diameter of the CCD detector was 13.5 cm. The sample-to-detector distance was 60 cm. The detector was offset horizontally to allow for high q acceptance.

the water reservoir. The chamber was covered by a double-layered insulating wall with kapton windows for the passage of x rays. Between the two layers a resistive heating coil maintained the surface temperature of the chamber above that of the sample so as to avoid water condensation on the kapton windows.

This compact temperature-humidity chamber, only ~7 cm on each side, was mounted on a small *x*-*z* rotary stage. The position of the sample chamber was carefully aligned to ensure that the beam and the sample surface intersected at the rotational axis of the rotary stage. The vertical position of the sample was separately adjustable so that different parts of the sample could be exposed to x rays. This was used to avoid radiation damage to the sample.

Data collection

Aligned lipid multilayers are ordered in the direction perpendicular to the substrate surface but randomly oriented in the plane parallel. Thus the crystal domains in such a sample have a crystal plane parallel to the substrate, whereas the in-plane orientations of the crystal domains are isotropically distributed. Consequently, in the reciprocal space, the lattice points are distributed in a series of Bragg rings parallel to the substrate and centered around the q_z axis. ($\boldsymbol{q}$ is the momentum transfer of x-ray scattering; z is normal to the plane of substrate, $\boldsymbol{r}$ or (x, y) are in-plane coordinates.) Each Bragg ring will be registered as a diffraction peak on the q_z-q_r plane, where q_r is the in-plane radius of the Bragg ring. We used a combination of three CCD images to record a complete diffraction pattern.

Supramolecular lipid structures have a length scale of 50–300 Å, and their diffraction peaks tend to be limited within <1 Å^{-1}. With x rays of 8 keV ($\lambda = 1.55$ Å) incident at a grazing angle (almost parallel to the substrate), the Ewald sphere intercepted the majority of the Bragg rings (recorded as *CCD image 1* in Fig. 2), but with two exceptions. First, the Bragg rings with $q_z = 0$ were inaccessible by reflection, because in practice reflection always imparted a finite q_z. These $q_z = 0$ Bragg peaks were recorded by transmission diffraction at an incident angle –30° (*CCD image 3* in Fig. 2). Second, at a fixed incident angle, the Ewald sphere intersected the q_z axis twice: one at the origin of reciprocal space and another at the specular angle. Therefore, the diffraction pattern by a grazing incident angle did not include the complete series of the q_z peaks (peaks with $q_r = 0$). These $q_r = 0$ peaks were measured by a θ-scan, in which the sample was rotated continuously to vary the incident angle, so that the intercept of the Ewald sphere with the q_z axis moved along this axis and recorded as CCD image 2 (Fig. 2). These three CCD images were combined to give a complete diffraction pattern.

The intensities of the diffraction peaks were integrated directly from the CCD image in the following manner. The peaks were first integrated in the direction of q_r (or q_z) over a width slightly wider than the apparent peak widths. The result was plotted along the q_z (or q_r) axis. On this one-dimensional profile, the background was obtained by using the intensities between the peaks and extrapolated into the peak regions. After subtracting the background, each peak was integrated along the direction of q_z (or q_r) axis.

Data reduction

The data collected above were used to obtain the amplitude of the form factor for the unit cell, F, at the positions of the Bragg peaks. In addition to the correction factors, we paid special attention to the (relative) normalization of the three CCD images.

The integrated intensity of a diffraction peak E measured in the reflection or the transmission geometry is related to the square of the form factor $|F|^2$ by

$$E = I_o |F|^2 C_p C_L C_{abs} C_{geo} \Delta T. \quad (1)$$

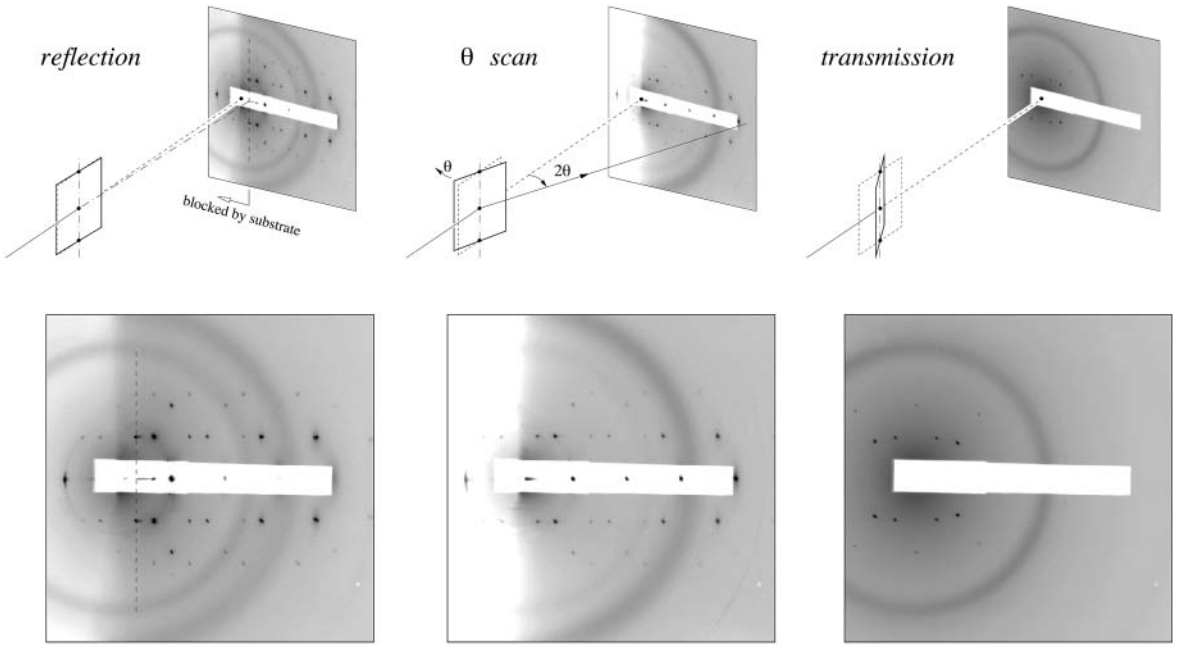

FIGURE 2 A complete diffraction pattern for the rhombohedral phase was obtained by a combination of three CCD recordings. (*A*) Reflection. X-ray beam was incident at a grazing angle (0.7°) to the substrate. In the CCD image, the region to the left of the dashed line was blocked by the silicon frame of the substrate. The spot between the dashed line and (001) was the specular reflection. (*B*) θ-scan. This was a conventional θ–2θ scan along the q_z axis. The intensities accumulated during the θ-scan at the peak positions off the q_z axis were not suitable for analysis. (*C*) Transmission. The incident angle was $-30°$. Each CCD image was the average of two 120 s exposures. The white strip in each image was the shadow of an x-ray attenuator. The dark rings were due to the kapton windows on the vacuum pipes and the sample chamber.

I_o is proportional to the incident beam intensity. Synchrotron radiation is usually linearly polarized. The polarization factor is determined by the angle between the incident polarization vector and the scattered beam, ψ: $C_p = \sin^2\psi$. The Lorentz factor is given by

$$C_L = \frac{1}{\cos\alpha\cos\nu\sin\gamma}, \tag{2}$$

where α is the x-ray incident angle with the substrate surface (the x-y plane), ν is the angle between the scattering vector $\boldsymbol{q}$ and the x-y plane, and γ is the angle between the in-plane (x-y) projection of $\boldsymbol{q}$ and the in-plane projection of the incident vector. The Lorentz factor is well known in x-ray crystallography (Kasper and Lonsdale, 1967), where a single crystal is rotated so that multiple diffraction peaks can be recorded. In the case of aligned lipid multilayers, the isotropic distribution of the in-plane orientation of the crystalline domains is equivalent to an in-plane rotation of a single crystal. The absorption factor is determined by the path length of the diffracted x-ray through the sample (Yang et al., 1998). For transmission diffraction, we have

$$C_{abs} = e^{-\mu a/\cos\omega}\frac{1-\exp\left[-\mu a\left(\frac{1}{\cos\beta}-\frac{1}{\cos\omega}\right)\right]}{\mu a\cos\omega\left(\frac{1}{\cos\beta}-\frac{1}{\cos\omega}\right)}, \tag{3}$$

and for reflection diffraction

$$C_{abs} = \frac{1-\exp\left[-\mu a\left(\frac{1}{\cos\beta}+\frac{1}{\cos\omega}\right)\right]}{\mu a\cos\omega\left(\frac{1}{\cos\beta}+\frac{1}{\cos\omega}\right)}, \tag{4}$$

where ω is the angle between the substrate normal and the incident beam ($0 < \omega < \pi/2$). β is the angle between the substrate normal and the scattered beam. μ is the linear absorption coefficient of the sample, and a is the sample thickness. The amount of sample that was bathed in the x ray and thus contributed to diffraction depended on the incident angle. This is taken into account by the factor

$$C_{geo} = \frac{b/\sin\alpha}{w} \quad \text{or} \quad 1 \text{ if greater than } 1, \tag{5}$$

where w is the horizontal width of the sample and the footprint of the incident beam of width b (0.5 mm) is $b/\sin\alpha$. ΔT is the exposure time.

For θ-scan, the integrated intensity of a diffraction peak is given by

$$E = I_o|F|^2 C_p C_L C_{abs} C_{geo}\frac{2\pi}{\Omega}, \tag{6}$$

where $C_p = \cos^2 2\theta$, and $C_L = 1/\sin 2\theta$. The absorption factor is given by $C_{abs} = [1-\exp(-2\mu a/\sin\theta)]/2\mu a$. The geometric factor C_{geo} is the same as Eq. 5. The last factor $2\pi/\Omega$ is the normalization factor relative to the exposure time for the reflection scan, with Ω being the angular velocity of the θ-scan.

One can also view the θ-scan as a special case of the reflection diffraction, with $\beta = \omega = \pi/2 - \theta$, $\alpha = \nu = 0$, $\gamma = 2\theta$ and the crystal rotation about the q_x axis instead of the q_z axis. Then all the correction factors are the same between Eq. 1 and Eq. 6.

RESULTS AND ANALYSIS

Phase diagram of DPhPC

DPhPC multilayers prepared in high humidities showed a single series of Bragg peaks in q_z. There were no diffraction peaks outside of q_z axis (Fig. 3 *A*). This phase is conventionally labeled as L_α. The sample was then housed in a chamber of controlled temperature and relative humidity (*RH*). Two other phases were identified in the range of temperature and *RH* shown in Fig. 3. Fig. 3 *B* shows the diffraction pattern of a rhombohedral lattice. Fig. 3 *C* shows a two-dimensional hexagonal lattice. The latter is the well-known inverted hexagonal (H_{II}) phase. In the past, the H_{II} phase was typically recorded by the method of powder diffraction, which produced a series of diffraction circles (Gruner, 1989; Turner and Gruner, 1992). Here the diffraction pattern shows a hexagonal lattice normal to the substrate, indicating that the H_{II} tubes were all oriented parallel to the substrate surface. The dimensions of the unit cell in the rhombohedral phase were ~65 Å (one side of the

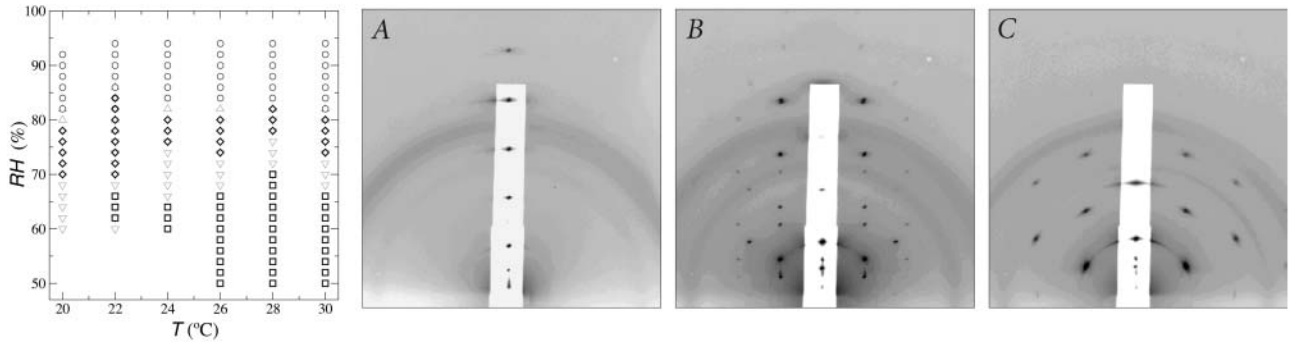

FIGURE 3 Phase diagram of lipid DPhPC as a function of temperature and the level of hydration measured by the ambient relative humidity (*RH*). The symbols circle, diamond, and square correspond to the x-ray diffraction patterns A, B, and C, respectively, shown on the right-hand side. Symbols Δ and ∇ indicate changeover regions where two phases were detected. The range of the changeover region depended on the direction of hydration change and the speed of the change. The x-ray diffraction patterns were recorded by reflection on an area detector (see Data collection and Fig. 2), where the ordinate was normal to the substrate surface. (The incident angle was 0.7° relative to the substrate.) The abscissa was proportional to the magnitude of the in-plane component of the reciprocal vector (approximately). (*A*) Diffraction pattern of a lamellar structure corresponding to the L_α phase. (*B*) Diffraction pattern of a rhombohedral structure (space group $R\bar{3}$). (*C*) Diffraction pattern of a two-dimensional hexagonal structure (space group p6) corresponding to the inverted hexagonal (H_{II}) phase.

hexagon) and ~44 Å (stack spacing). The unit cell in the two-dimensional hexagonal phase was ~41 Å for each side of the hexagon. These dimensions varied somewhat with the degree of hydration.

The phase diagram was obtained by varying RH at constant temperature. The changeover regions showed diffraction patterns of two phases, probably the result of a long relaxation time during the phase change. As shown in the phase diagram, the phase transitions were mainly due to hydration change. The temperature dependence between 20° to 30°C was rather weak. Notice that the rhombohedral phase covered a range of humidity from ~70% to ~80%RH. This hydration dependence will be utilized for phase determination.

Swelling method in three dimensions

Phase determination for the diffraction of the L_α phase (Fig. 3 *A*) is often accomplished by the swelling method (Bragg and Perutz, 1952; Perutz, 1954; Blaurock, 1971). This method takes advantage of the hydration changes of the layer system that alter the stacking distance while the bilayer structure remains approximately the same (Torbet and Wilkins, 1976). If the bilayer is symmetric, the phases are real, either positive or negative. Then the form factor of the bilayer is a continuous, real function of q_z that changes sign only when it goes through zero. The variation of the stacking distance covers a short range of q_z at every peak position. Thus a series of diffraction patterns over a range of hydration often provide sufficient information to determine the phases as in the case of DPhPC (Fig. 4). Once the phases were determined, the diffraction patterns of the L_α phase were used to construct the trans-bilayer electron density profiles.

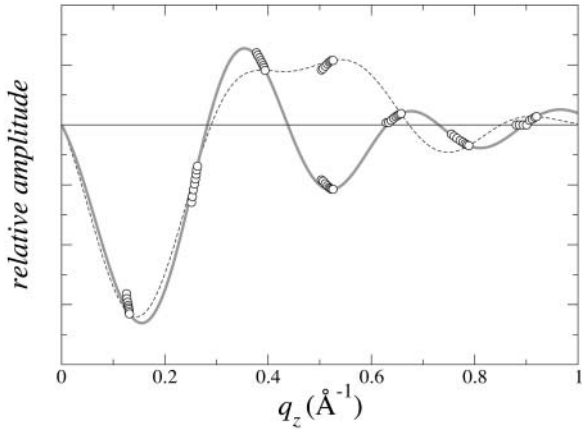

FIGURE 4 One-dimensional swelling method for phase determination applied to the L_α phase of DPhPC. The normalized diffraction amplitudes for a series of varying degrees of hydration are plotted as a function of q_z. Each amplitude takes either positive or negative sign. The choice of the phases must be such that the constructed form factor $F(q_z)$ goes through all the data points. The choice indicated by the solid line (which is the $F(q_z)$ constructed from one set of data) meets the criterion, whereas the choice indicated by the dotted line does not.

These profiles of the L_α phase will be compared with the trans-bilayer profiles in the rhombohedral phase.

We now show that the swelling method can be extended to a layered system containing in-plane structures. For an example, we consider rhombohedral structures. We start with the form factor of the unit cell $F(\boldsymbol{q})$ and the diffraction amplitude $A_{\mathrm{H,\,K,\,L}}$:

$$F(\boldsymbol{q}) = \iiint_{\mathrm{unit-cell}} \Delta\rho(r)\cos(\boldsymbol{q}\cdot\boldsymbol{r})d^3r \quad \text{and } A_{\mathrm{H,K,L}} = F(\boldsymbol{q}_{\mathrm{H,K,L}}), \tag{7}$$

where we use the hexagonal indices H,K,L for the reciprocal lattice points. Because the zeroth order ($\boldsymbol{q} = 0$) diffraction peak is not measurable, the form factor is determined by the electron density contrast $\Delta\rho$ rather than the electron density ρ itself. We have also assumed that the unit cell is centrosymmetric. The purpose of the diffraction experiment is to measure the magnitudes of the diffraction amplitudes $A_{\mathrm{H,\,K,\,L}}$ and then determine their phases, so that the electron density contrast can be constructed:

$$\Delta\rho(\boldsymbol{r}) = \frac{1}{V}\sum_{\mathrm{H,K,L}} A_{\mathrm{H,K,L}}\cos(\boldsymbol{q}_{\mathrm{H,K,L}}\cdot\boldsymbol{r}), \tag{8}$$

where V is the volume of the unit cell. Substitution of Eq. 8 to Eq. 7 leads to:

$$F(\boldsymbol{q}) = \frac{1}{2V}\sum_{\mathrm{H,K,L}} A_{\mathrm{H,K,L}}\iiint_{\mathrm{unit-cell}}\{\cos[(\boldsymbol{q}-\boldsymbol{q}_{\mathrm{H,K,L}})\cdot\boldsymbol{r}] + \cos[(\boldsymbol{q}+\boldsymbol{q}_{\mathrm{H,K,L}})\cdot\boldsymbol{r}]\}d^3r. \tag{9}$$

We now separate the vectors into their in-plane and out-of-plane components, i.e., $\boldsymbol{q} = \boldsymbol{q}_\mathrm{r}+q_z\hat{z}$, $\boldsymbol{r} = \boldsymbol{r}_2+z\hat{z}$, $q_{\mathrm{H,K,L}} = q_{\mathrm{H,K}}+q_\mathrm{L}\hat{z}$ and carry out the spatial integration over z from $-$d/2 to d/2 (d is the stacking distance) to obtain

$$F(\boldsymbol{q}) = \frac{d}{2V}\sum_{\mathrm{H,K,L}} A_{\mathrm{H,K,L}}\left\{C^{+}_{\mathrm{H,K}}(\boldsymbol{q}_\mathrm{r})\mathrm{sinc}\left[\frac{d}{2}(q_z+q_\mathrm{L})\right] + C^{-}_{\mathrm{H,K}}(\boldsymbol{q}_\mathrm{r})\mathrm{sinc}\left[\frac{d}{2}(q_z-q_\mathrm{L})\right]\right\}, \tag{10}$$

with

$$C^{\pm}_{\mathrm{H,K}}(\boldsymbol{q}_\mathrm{r}) = \iint_{\mathrm{unit-cell}}\cos[(\boldsymbol{q}_\mathrm{r}\pm\boldsymbol{q}_{\mathrm{H,K}})\cdot\boldsymbol{r}_2]d^2r_2. \tag{11}$$

When $\boldsymbol{q}_r = \boldsymbol{q}_{\mathrm{H,K}}$, we have $(d/V)C^{\pm}_{\mathrm{H',K'}}(\boldsymbol{q}_{\mathrm{H,K}}) = \delta_{\mathrm{H},\mp\mathrm{H}'}\delta_{\mathrm{K},\mp\mathrm{K}'}$ and therefore, we obtain

$$F(\boldsymbol{q}_{\mathrm{H,K}}, q_z) = \frac{1}{2}\sum_\mathrm{L}\left\{A_{-\mathrm{H},-\mathrm{K,L}}\,\mathrm{sinc}\left[\frac{d}{2}(q_z+q_\mathrm{L})\right] + A_{\mathrm{H,K,L}}\,\mathrm{sinc}\left[\frac{d}{2}(q_z-q_\mathrm{L})\right]\right\} = \sum_L A_{\mathrm{H,K,L}}\,\mathrm{sinc}\left[\frac{d}{2}(q_z-q_\mathrm{L})\right]. \tag{12}$$

The second equality is due to the assumed centro-symmetry of the unit cell. This is the equation for constructing the form

factor as a continuous function of q_z from a single set of diffraction peaks. If the form factor $F(\boldsymbol{q}_{H,K},q_z)$ varies slowly and continuously with hydration, Eq. 12 can be used to help determine the phases, that is, $F(\boldsymbol{q}_{H,K},q_z)$ constructed from any set of diffraction peaks should have the q_z-dependence approximately the same as the q_z-dependence of the real data caused by the hydration change (Torbet and Wilkins, 1976). To normalize the diffraction amplitudes between different sets of data, we note that

$$\int_{-\infty}^{\infty} |F(\boldsymbol{q}_{H,K}, q_z)|^2 dq_z = \frac{2\pi}{d}\sum_L A^2_{H,K,L}, \qquad (13)$$

due to the orthogonality of the sinc functions. The left-hand side of Eq. 13 is approximately a constant if the change of the form factor with hydration is relatively small. Thus for the purpose of phase determination, the diffraction amplitudes for each data set will be normalized by making $\sum_L A^2_{H,K,L}$ proportional to its stacking distance d.

Phase determination and electron density distribution in the unit cell

As mentioned above, every diffraction peak with $\boldsymbol{q}_{H,K} > 0$ is distributed on a Bragg ring around the z axis. Peaks with the same $q_r = \sqrt{q_x^2+q_y^2}$ and q_z overlapped in the same ring, so they were assumed to have the same diffraction amplitude. Fig. 5 shows the reciprocal lattice and the diffraction peaks measured on the q_z-q_r plane. The reciprocal lattice of rhombohedral symmetry is composed of a stack of hexagonal layers stacked up in the ABCABC. . . sequence. Fig. 5 shows A layers as green, B as blue and C as red. In the q_z-q_r plane, we showed the four columns of the observed diffraction peaks. The spacing for each color in each column is 2π/d. The occupied positions on q_z depend on the values of (H, K). In column a and c, the green peaks are at nq_z^o (n = 0, ±1, ±2,. . .; $q_z^o = 2\pi$/d), and in column b and d, blue peaks occupy $(n + 1/3)q_z^o$, and red peaks occupy $(n - 1/3)q_z^o$. On the detector (Figs. 2 and 3), the blue peaks and the red peaks were mixed because domains of both +z and −z orientations were equally populated in the sample. The mixed blue and red peaks were, however, the same under the assumption of centro-symmetry. The multiplicities for the diffraction peaks at $q_r/q_r^o = 0,1,\sqrt{3},2$ are 1, 3, 6, and 3, respectively, where q_r^o is the magnitude of the lowest in-plane component q_r from the peaks on the first column off the q_z axis (*column b* in Fig. 5).

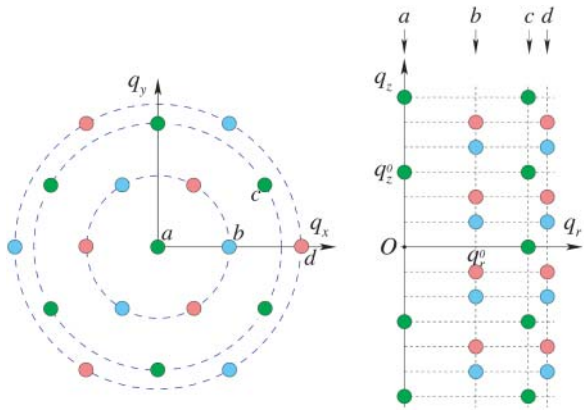

FIGURE 5 The reciprocal lattice of rhombohedral symmetry on the q_x-q_y plane and the diffraction peaks detected on the q_z-q_r plane. The reciprocal lattice of rhombohedral symmetry is composed of a stack of hexagonal layers stacked up in the ABCABC. . . sequence (A green, B blue, C red). In the q_z-q_r plane are the four columns of the observed diffraction peaks. In Fig. 6, the swelling method was applied to each set of the peaks having the same (H,K) (same color): column a ($H = 0$,$K = 0$), b (1,0), c(1,1), and d(2,0). The set of red peaks and the set of blue peaks in each of column b and d are equivalent by centro-symmetry.

We now apply the swelling method to each q_z line in the rhombohedral lattice (Fig. 5, *left*), equivalently, the peaks of the same color in each column in the q_z-q_r plane (Fig. 5, *right*). Diffraction patterns were collected from a DPhPC sample at 28°C for four different relative humidities: 79%, 77.5%, 76%, and 74.5%. The corrected amplitudes (see Data reduction) are listed in Table 1 where the amplitudes for different relative humidities have been relatively normalized according to Eq. 13. The swelling-form factor diagrams are shown in Fig. 6. The solid curve in each swelling diagram was the construction Eq. 12 from one set of data. We note

TABLE 1 Corrected diffraction amplitudes at four hydration levels

(q_r/q_r^0, $3q_z/q_z^0$)	Dataset 1 q_r^0 = 0.1060 Å^{-1} q_z^0 = 0.1414 Å^{-1}	Dataset 2 q_r^0 = 0.1095 Å^{-1} q_z^0 = 0.1422 Å^{-1}	Dataset 3 q_r^0 = 0.1108 Å^{-1} q_z^0 = 0.1428 Å^{-1}	Dataset 4 q_r^0 = 0.1121 Å^{-1} q_z^0 = 0.1435 Å^{-1}
(0, 3)	6.2389	6.1779	6.0459	6.0417
(0, 6)	0.9767	0.9339	0.8860	0.8417
(0, 9)	1.3068	1.2797	1.2382	1.2051
(0, 12)	0.8224	0.8272	0.8028	0.7752
(0, 15)	0.2605	0.2628	0.2570	0.2526
(0, 18)	0.2210	0.2121	0.1719	0.1572
(1, 1)	0.9157	0.9800	0.9944	1.0059
(1, −2)	1.5629	1.5938	1.4778	1.4384
(1, 4)	0.2297	0.2166	0.2019	0.1922
(1, −5)	0.2704	0.2560	0.2464	0.2244
(1, 7)	0.1089	0.1117	0.1048	0.0992
(1, −8)	0.4927	0.4832	0.4843	0.4815
(1, −11)	0.5740	0.5628	0.5585	0.5490
(1, −14)	0.0973	0.1034	0.1066	0.1096
(1, −17)	0.1359	0.1319	0.1290	0.1269
($\sqrt{3}$, 0)	0.3596	0.3468	0.3458	0.3322
($\sqrt{3}$, 3)	0.3079	0.3099	0.3038	0.3036
($\sqrt{3}$, 6)	0.1072	0.1171	0.1260	0.1316
($\sqrt{3}$, 12)	0.0728	0.0663	0.0635	0.0622
(2, −2)	0.1443	0.1303	0.1241	0.1224
(2, 4)	0.1686	0.1590	0.1598	0.1616
(2, 7)	0.1670	0.1731	0.1809	0.1902
(2, 10)	0.1448	0.1533	0.1626	0.1766

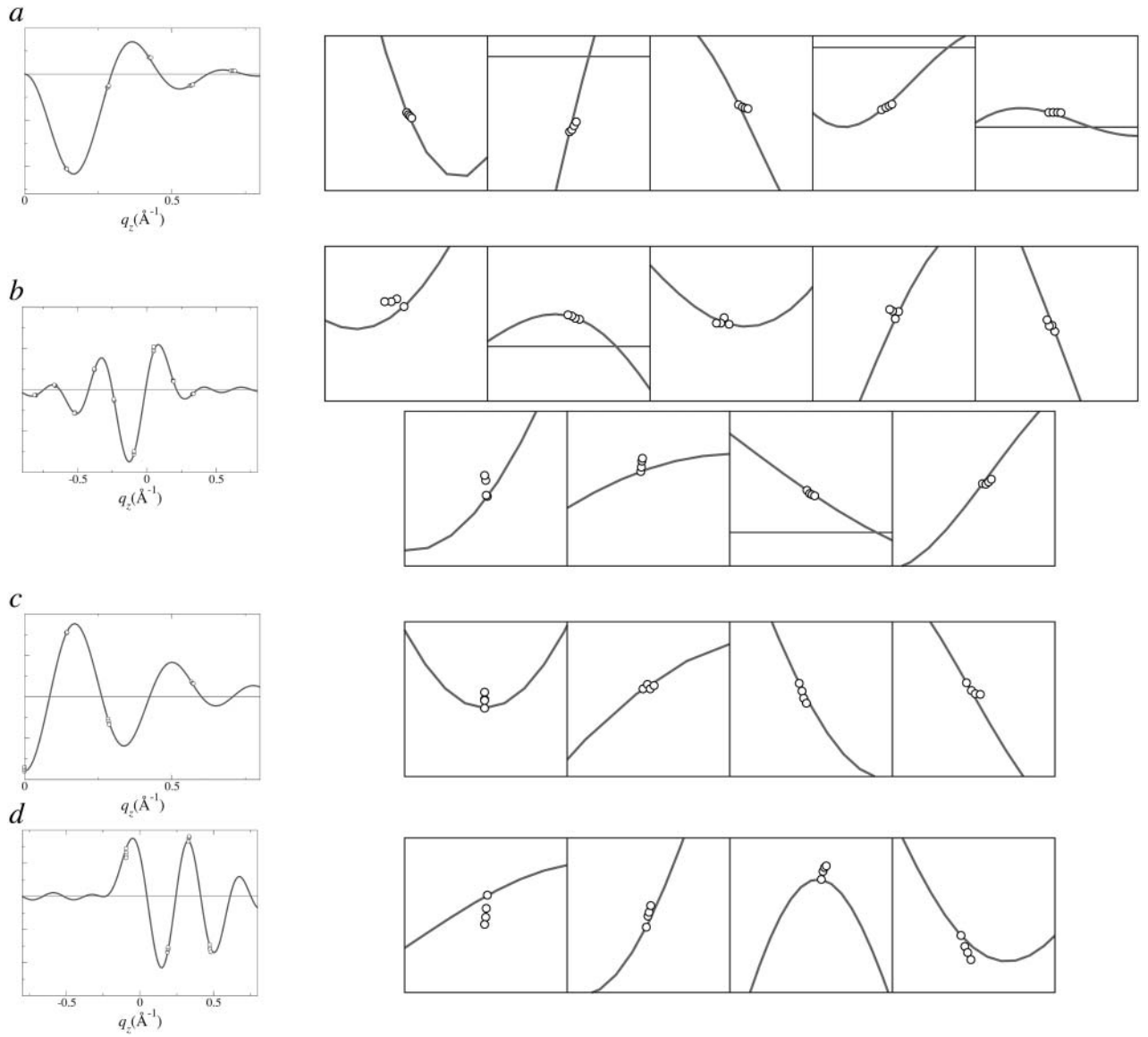

FIGURE 6 Three-dimensional swelling method for phase determination applied to the rhombohedral phase. The panels on the left show the swelling method applied to each column *a*, *b*, *c*, *d*, (indicated in Fig. 5) using the diffraction amplitudes from Table 1. The vertical scales are relative. The solid curves are $F(\boldsymbol{q}_{H,K}, q_z)$of Eq. 12 constructed from one set of data measured at one relative humidity. For each panel on the left, the curve and data points were magnified to show the effect of swelling (one to one correspondence from left to right; the second row follows the first row for panel *b*).

that the range of swelling is not as wide as in the L_α phase shown in Fig. 4. Nevertheless, for the majority of the lattice points we could choose the phases so that the q_z-dependence of the data was consistent with that of the constructed $F(\boldsymbol{q}_{H,K},q_z)$. The phases shown in Fig. 6 are the best choices according to the swelling method. The choices are also consistent with the minimum wavelength principle. This principle was introduced by Bragg and Perutz (Bragg and Perutz, 1952; Perutz, 1954) as an aid to the swelling method. They showed that whatever the arrangement of the scattering points in the structure, the maxima and minima of the form factor succeed each other with a minimal wave number dictated by the overall dimensions of the molecule in a corresponding direction. In our case, the minimal wave number for the q_z dependence should correspond to the thickness of the layers of the rhombohedral structure, which is about that of a bilayer as compared with the L_α phase. Independently, the phases for the lamellar structure shown in Fig. 4 apparently satisfy the minimum wavelength principle.

After the relative phases within each column (of Fig. 5) were determined, there were 2^3 (8) possible choices for the relative phases between the four columns. We can narrow the choices by using a pattern recognition method proposed by Luzzati and his collaborators (Mariani et al., 1988 and references therein). This method recognizes the fact that the basic structural element of lipid in water is the lipid

monolayer. A change of the structure of a lipid-water system is a rearrangement of the lipid monolayers (Tardieu et al., 1973). Therefore, if a lipid-water system has more than one structure, the different structures should have comparable electron density contrast histograms $H(\Delta\rho)$. For example, the structure of DPhPC in the L_α phase was known (Hung et al., 2000) and was reconstructed here, so its $H(\Delta\rho)$ could be used as a reference. For the rhombohedral phase we computed $H(\Delta\rho)$ for each of the eight possible choices of relative phases and compared the results with that of the L_α phase. For practical purposes, the method was carried out by computing the fourth moment $\langle(\Delta\rho)^4\rangle$ following the procedure of Mariani et al., 1988:

$$\left\langle(\Delta\rho)^4\right\rangle = \frac{\sum_{H,K,L}\left|\sum_{H',K',L'} F(\boldsymbol{q}_{H'-H,K'-K,L'-L})F(\boldsymbol{q}_{H',K',L'})\right|^2}{\left(\sum_{H,K,L}|F(\boldsymbol{q}_{H,K,L})|^2\right)^2}. \quad (14)$$

Among the eight possible choices (Fig. 7), two with $\langle(\Delta\rho)^4\rangle = 2.610$ and 2.640 are closest to the value of the L_α phase which has $\langle(\Delta\rho)^4\rangle = 1.750$. The electron density distributions of these two choices (*3* and *7* in Fig. 7) are very similar, both show a stalk structure. However, upon close inspection, we found that choice 3 produced somewhat uneven electron densities in the lipid headgroup region along the monolayers. The most reasonable choice of phases (*7* of Fig. 7) gave the electron density distribution shown in Fig. 8. Other details were shown in Yang and Huang (2002).

DISCUSSION

Ultimately the choice of phases is justified for producing a rational electron density distribution. For lipid-water systems, the electron density distribution must satisfy the expected properties of lipid in water, that is, there should be continuous monolayers with the high-density headgroup regions facing low-density water regions, and low-density chains regions surrounded by high-density headgroup regions. Our result is consistent with these expected properties (see the electron density profiles along three different cuts shown in the *upper right panel* of Fig. 8). The electron density profile of the bilayer region in the rhombohedral phase (shown as *cut a*) remained very close to the bilayer profile of the L_α phase. On the contrary, examples of irrational results can be seen in the choice 0, 1, 2, 4, 5, and 6 in Fig. 7 where the electron density distributions are not consistent with the expected properties of lipid in water as described.

The electron density distribution shows a structure similar to the theoretically expected stalk structure (Gingell and Ginsberg, 1978; Markin et al., 1984; Siegel, 1993), namely, the two apposed monolayers apparently merged and bent into an hourglass shape. This structure has been speculated to be an intermediate state during membrane fusion. It has also been speculated that stalks are the intermediate state between the lamellar phase and the inverted hexagonal phase (Siegel, 1999). However, the stalk (rhombohedral) phase was not observed in previous studies of lamellar to inverted hexagonal transitions (Gawrisch et al, 1992). Apparently a direct transition between any two of the lamellar, stalk, and H_{II} phases is possible.

The discovery of the putative membrane fusion intermediate state in a stable phase is significant. It not only lends a strong support to the stalk hypothesis for membrane fusion, but also opens a new experimental approach to the fusion problem. Firstly we should now try to enhance the resolution of the diffraction to improve the measurement of the structural parameters that characterize a stalk structure. This includes a possible refinement of the experimental setup and possible modifications of the contrast between the headgroup and the hydrocarbon chains by multiwavelength diffraction or other means. Secondly we can vary the lipid composition

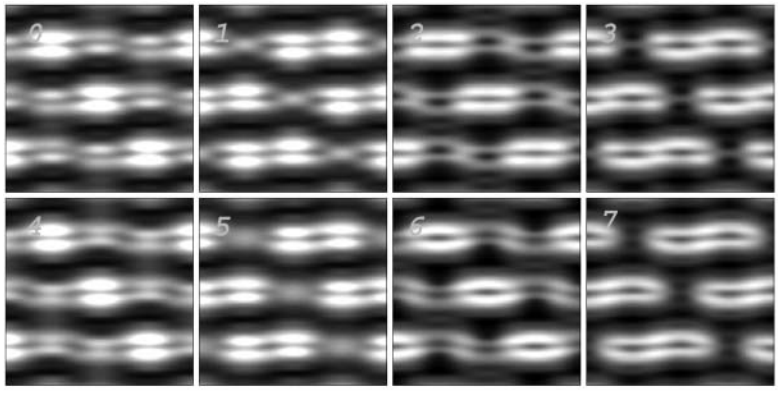

	relative phase	$\langle(\Delta\rho)^4\rangle$
0	++++	4.163
1	+-++	3.625
2	++-+	3.013
3	+--+	2.610
4	+++-	4.416
5	+-+-	3.550
6	++--	3.063
7	+---	2.640

FIGURE 7 $\langle(\Delta\rho)^4\rangle$ for the eight possible choices of relative phases are shown in the table on the right. The corresponding electron density maps are shown on the left. The choice 3 and 7 are closest to the value of the L_α phase which has $\langle(\Delta\rho)^4\rangle = 1.750$. The electron density maps of choice 3 and 7 are very similar, both showing a stalk structure. However, upon close examination, the electron density map of the choice 3 shows somewhat uneven densities for the lipid headgroup along the lipid monolayer (not obvious from the map). Therefore, the choice 7 is considered the most reasonable.

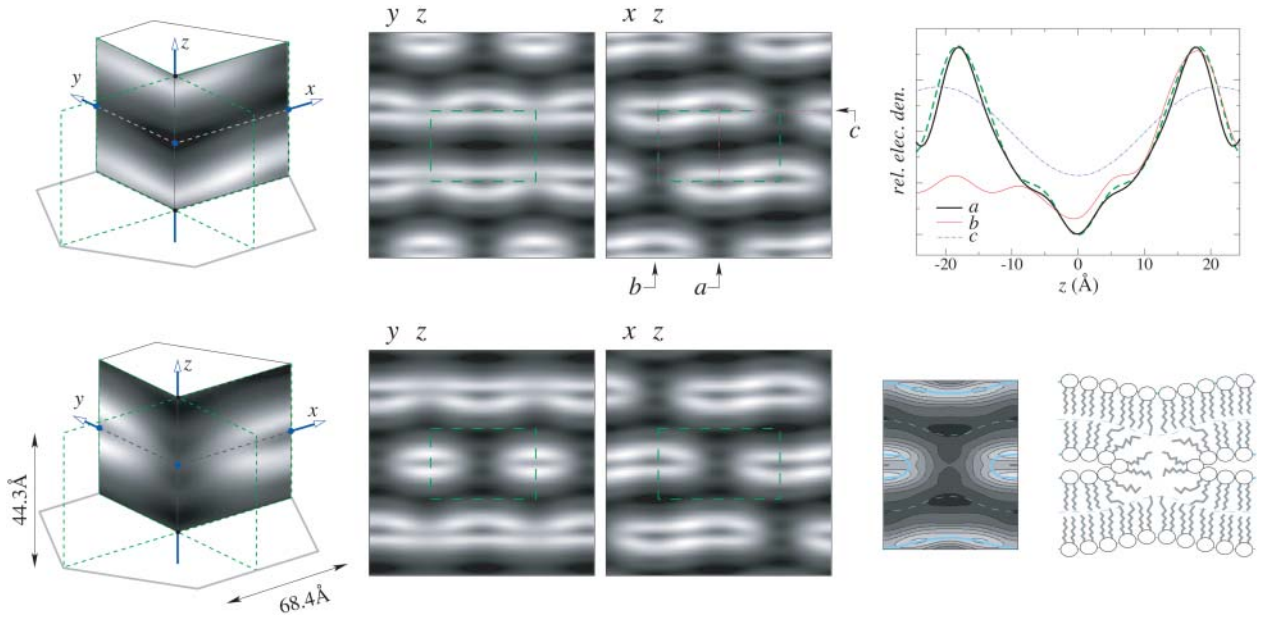

FIGURE 8 Electron density distribution in the unit cell of the rhombohedral lattice. (High density is white, low density is black.) (*Top row*) The unit cell was based on the phases determined by the swelling and pattern recognition methods. The stalk structure is not obvious in this unit cell. To its right are the density maps in the *y*-*z* and *x*-*z* planes. The dashed green rectangles are the boundaries of the unit cell in each map. On the *x*-*z* map, the electron density profiles were taken along three lines a, b, and c, and shown in the top right panel. Also shown in the panel is a trans-bilayer density profile from the L_α phase. The bilayer portion in the rhombohedral phase remained very close to the L_α phase. (*Bottom row*) The unit cell was obtained by a translation from the previous one. A stalk structure appeared at the center of the cell. The maps on the *y*-*z* and *x*-*z* planes are shown to its right. The central part of the *y*-*z* map is replotted with density contours on the right hand side, along with a cartoon of a stalk where two lipid monolayers merged to form a hourglass structure.

and include fusogenic peptides or other chemical variables in the system to observe their effects on the stalk structure. In the last 10 years, significant progress has been made in the elucidation of the structures of membrane fusion proteins (White, 1992; Brunger, 2001). However, how proteins induce membrane fusion remains speculative, even in the best-studied case of viral fusion proteins (White, 1992; Doms, 1993; Stegmann, 1994; Chernomordik et al., 1997). Direct studies of the intermediate state will help clarifying the free energy pathway for the lipid conformation changes during fusion. This information will in turn provide guidance to identify the functions of the protein structures.

In our previous investigations, we have shown that lipids bilayers containing peptides initially prepared in the lamellar phase often developed into a rhombohedral phase by temperature and hydration manipulation (Yang et al., 2000). The technique described here allows the peptide-induced membrane structures to be studied by x-ray and neutron diffraction. The swelling method should be helpful for the phase problem in such experiments.

We thank W. A. Caliebe for his assistance in setting up the diffraction experiment.

This work was supported by NIH Grants GM55203 and RR14812, and by the Robert A. Welch Foundation. Research carried out in part at the beamline X21 of the National Synchrotron Light Source, Brookhaven National Laboratory, which is supported by the U.S. Department of Energy, Division of Materials Sciences and Division of Chemical Sciences, under Contract No. DE-AC02-98CH10886.

REFERENCES

Blaurock, A. E. 1971. Structure of the nerve myelin membrane: proof of the low resolution profile. *J. Mol. Biol.* 56:35–52.

Bragg, L., and M. F. Perutz. 1952. The structure of hemoglobin. *Proc. R. Soc. Lond. A.* 213:425–435.

Brunger, A. T. 2001. Structural insights into the molecular mechanism of calcium-dependent vesicle-membrane fusion. *Curr. Opin. Struct. Biol.* 11:163–173.

Chernomordik, L. V., E. Leikina, V. Frolov, P. Bronk, and J. Zimmerberg. 1997. An early state of membrane fusion mediated by the low pH conformation of influenza hemagglutinin depends upon membrane lipids. *J. Cell Biol.* 136:81–93.

Doms, R. W. 1993. Protein conformational changes in virus-cell fusion. *Methods Enzymol.* 221:61–72.

Gawrisch, K., V. A. Parsegian, D. A. Hajduk, M. W. Tate, S. M. Gruner, N. L. Fuller, and R. P. Rand. 1992. Energetics of a hexagonal-lamellar-hexagonal-phase transition sequence in dioleoylphosphatidyl ethanolamine membranes. *Biochemistry.* 31:2856–2864.

Gingell, D., and I. Ginsberg. 1978. Problems in the physical interpretation of membrane interaction and fusion, *In* Membrane Fusion, G., Post, G. L., Nicholson, Eds. Elsevier, Amsterdam. 791–833.

Gruner, S. M. 1989. Stability of lyotropic phases with curved interfaces. *J. Phys. Chem.* 93:7562–7570.

He, K., S. J. Ludtke, D. L. Worcester, and H. W. Huang. 1995. Antimicrobial peptide pores in membranes detected by neutron in-plane scattering. *Biochemistry.* 34:15614–15618.

He, K., S. J. Ludtke, D. L. Worcester, and H. W. Huang. 1996. Neutron scattering in the plane of membrane: structure of alamethicin pores. *Biophys. J.* 70:2659–2666.

Huang, H. W. 2000. Action of antimicrobial peptides: Two-state model. *Biochemistry*. 39:8347–8352.

Hung, W. C., F. Y. Chen, and H. W. Huang. 2000. Order-disorder transition in bilayers of diphytanoyl phosphatidylcholine. *Biochim. Biophys. Acta*. 1467:198–206.

Kasper, J., and K. Lonsdale. eds. 1967. *International Table for X-ray Crystallography. Vol. II*. Kynoch Press, Bringham, England. 237–267.

Kittel, C. 1971. Introduction to Solid State Physics. 4th Ed. John Wiley, New York. 28–29.

Kozlovsky, Y., and M. M. Kozlov. 2002. Stalk model of membrane fusion: solution of energy crisis. *Biophys. J.* 82:882–895.

Kuzmin, P. I., J. Zimmerberg, Y. A. Chizmadzhev, and F. S. Cohen. 2001. A quantitative model for membrane fusion based on low-energy intermediates. *Proc. Natl. Acad. Sci. USA*. 98:7235–7240.

Lentz, B. R., V. Malinin, M. E. Haque, and K. Evans. 2000. Protein machines and lipid assemblies: current views of cell membrane fusion. *Curr. Opin. Struct. Biol.* 10:607–615.

Lentz, B. R., D. P. Siegel, and V. Malinin. 2002. Filling potholes on the path of fusion pores. *Biophys. J.* 82:555–557.

Ludtke, S., K. He, and H. W. Huang. 1995. Membrane thinning caused by magainin 2. *Biochemistry*. 34:16764–16769.

Ludtke, S. J., K. He, W. T. Heller, T. A. Harroun, L. Yang, and H. W. Huang. 1996. Membrane pores induced by magainin. *Biochemistry*. 35:13723–13728.

Mariani, P., V. Luzzati, and H. Delacroix. 1988. Cubic phases of lipid-containing systems: Structure analysis and biological implications. *J. Mol. Biol.* 204:165–189.

Markin, V. S., and J. P. Albanesi. 2002. Membrane fusion: stalk model revisited. *Biophys. J.* 82:693–712.

Markin, V. S., M. M. Kozlov, and V. L. Borovjagin. 1984. On the theory of membrane fusion. The stalk mechanism. *Gen. Physiol. Biophys.* 3: 361–377.

Perutz, M. F. 1954. The structure of haemoglobin. III. Direct determination of the molecular transform. *Proc. R. Soc. Lond. A*. 225:264–286.

Siegel, D. P. 1993. Energetics of intermediates in membrane fusion: comparison of stalk and inverted micellar intermediate mechanisms. *Biophys. J.* 65:2124–2140.

Siegel, D. P. 1999. The modified stalk mechanism of lamellar/inverted phase transitions and its implications for membrane fusion. *Biophys. J.* 76:291–313.

Stegmann, T. 1994. Anchors aweigh. *Curr. Biol.* 4:551–554.

Tardieu, A., V. Luzzati, and F. C. Reman. 1973. Structure and polymorphism of the hydrocarbon chains of lipids: a study of lecithin-water phases. *J. Mol. Biol.* 75:711–733.

Torbet, J., and M. H. F. Wilkins. 1976. X-ray diffraction studies of lecithin bilayers. *J. Theor. Biol.* 62:447–458.

Turner, D. C., and S. M. Gruner. 1992. X-ray diffraction reconstruction of the inverted hexagonal (H_{II}) phase in lipid-water systems. *Biochemistry*. 31:1340–1355.

White, J. M. 1992. Membrane fusion. *Science*. 258:917–924.

Yang, L., T. A. Harroun, W. T. Heller, T. M. Weiss, and H. W. Huang. 1998. Neutron off-plane scattering of aligned membranes I. Method of measurement. *Biophys. J.* 75:641–645.

Yang, L., T. M. Weiss, T. A. Harroun, W. T. Heller, and H. W. Huang. 1999. Supramolecular structures of peptide assemblies in membranes by neutron off-plane scattering: Method of analysis. *Biophys. J.* 77:2648–2656.

Yang, L., T. M. Weiss, R. I. Lehrer, and H. W. Huang. 2000. Crystallization of antimicrobial pores in membranes: magainin and protegrin. *Biophys. J.* 79:2002–2009.

Yang, L., and H. W. Huang. 2002. Observation of a membrane fusion intermediate structure. *Science*. 297:1877–1879.